Title: Immune and Clotting Dysfunction Detected in Saliva and Blood Plasma after COVID-19.

Running Title: *Salivary Detection of Early Immune Dysfunction in COVID-19*

Authors: Hyesun Jang[1], Saibyasachi Choudhury[2], Yanbao Yu[3], Benjamin L. Sievers[1], Terri Gelbart[1], Harinder Singh[1], Stephen A. Rawlings[4], Gene S. Tan[1,5], Davey Smith[5], Marcelo Freire[1,5]

[1] Genomic Medicine and Infectious Diseases, J. Craig Venter Institute, La Jolla, CA, and Rockville, MD, USA

[2] DGG-Genomics Division, Agilent, Technologies, Inc., La Jolla, CA 92037

[3] Department of Chemistry & Biochemistry, University of Delaware, Newark, DE, USA, 19716

[4] MMP Adult Infectious Disease, Maine Medical Center, South Portland, ME, 04106

[5] Division of Infectious Diseases and Global Public Health Department of Medicine, University of California San Diego, La Jolla, CA, USA

Corresponding Author:

Marcelo Freire, D.D.S., Ph.D., D.Med.Sc.
Associate Professor
Genomic Medicine and Infectious Diseases
J. Craig Venter Institute
4120 Capricorn Lane, La Jolla, CA 92037, USA
Phone: 858-200-1846
Fax: 858-200-1880
E-mail: mfreire@jcvi.org

ABSTRACT

It is becoming increasingly clear that individuals recovered from acute coronavirus disease 2019 (COVID-19) can develop into long-term sequelae (post-acute sequala of SARS-CoV-2 infection, PACS). While antibody response kinetics against viral particles is well studied in natural infection and vaccine, the molecular mechanisms governing disease formation remain elusive. We investigated plasma and saliva samples from COVID-19 and healthy control subjects to understand early immune responses globally after exposure to the virus. Antibody analyses showed robust IgA and IgG responses, neutralizing functions to the SARS-CoV-2, and positive correlations between matched plasma and saliva fluids. Shotgun proteomics revealed persistent inflammatory patterns in convalescent samples including dysfunction of neutrophil-fibrinogen axis, and dysregulated immune and clotting functions. Our study suggests saliva as fluid to monitor serology and immune functions to detect early and chronic signs of disease development. Further delineation of the pathophysiology in saliva may lead to discovery of novel biomarkers and therapeutic targets to patients at risk to develop PASC and chronic conditions.

Keywords: Saliva, COVID-19, SARS-CoV-2, chronic inflammation, secretory IgA, Clotting, Pathology, Proteomics, Post-acute sequelae of SARS-CoV-2 infection (PASC)

INTRODUCTION

The coronavirus disease 2019 (COVID-19), caused by severe acute respiratory syndrome coronavirus-2 (SARS-CoV-2), has had devastating impacts on global health [1,2]. Blood (*e.g.,* serum, plasma and peripheral mononuclear cells) and lungs of COVID-19 patients have been extensively investigated to reveal the acute phase immunopathogenesis and discover diagnostic and protective markers [3–6]. Of the blood components evaluated, the induction of antibodies and T cells play crucial roles in the neutralization and clearance of SARS-CoV-2 viruses, crucial to prevent the infection and reduce disease severity [7–9]. Also, the dysregulated neutrophil functions and blood clot process in the early infection phase has been reported to be associated with severe sequelae of COVID-19 [10–15].

As millions of people have been recovered from the SARS-CoV-2 infection, there have been an increasing number of long-term complications of the COVID-19[16,17]. Recent reports warrant that the immunopathogenesis of COVID-19 is beyond the acute-phase systemic or pulmonary disease (<2weeks). A recent case-control study of 31 individuals with post-acute sequalae of SARS-CoV-2 infection (PACS) found elevated levels of T cell immunoglobulin mucin domains and elevated cytokines in both PACS cases and non-PACS convalescent controls[18], suggesting a sustained inflammatory response were present independent of the clinical manifestation of the PASC. While millions of people are suffering from lingering symptoms after the COVID-19, even a clear diagnostic definition has not been established Early responses of immune dysfunction remain unknown and early factors to anticipate COVID-19 sequelae are needed[1920]. Understanding “how” and “why" inflammatory responses persist over multiple organs, is needed to detect the early signs and develop intervening strategies [4,21].

Inter-related multiple biological factors have been reported to be associated with the establishment of the PACS, including host immune dysregulation and dysbiosis in the microbiome

at mucosal surfaces [21–23]. It is now known that aberrant innate immune signaling cascades, resulting in a viscous loop of inflammation sustained after clearance of virus, drive the early stage to long-term actions[24]. Yet, the early drivers that govern molecular dysbiosis and tissue damage at the mucosal surface are not completely dissected. For a better understanding on the pathophysiology before PASC developers, a novel approach is needed to define normal vs. pathologic convalescent process and to detect initiation of aberrant innate immune activation, especially at mucosal surfaces that are in direct contact with the viral particles.

Saliva is an important vehicle for the silent spread of the SARS-CoV-2 viruses and a critical target to end the explosive transmission of the SARS-CoV-2 variants[25]. In addition, saliva is a practical and optimal target to monitor alterations of mucosal immune system by respiratory infection, as being: 1) a direct surrogate for antibody response derived from bronchial-alveolar lymphoid tissues (BALT) to the SARS-CoV-2 viral infection[26], 2) a reflection of systemic reactions to infection as more than 90% of body protein components are detected from saliva [27], 3) containing oral commensals which shape the host immune profile [28], and 4) oral inflammation can influence on the severity of systemic inflammatory responses [29–31]. Recent studies reported the association of the oral/gastrointestinal mucosal alterations with the pathophysiology of PASC [21,23,32], underpinning the potential of saliva to discover molecular mechanisms and early indicators.

This study was designed to capture the chronic inflammatory response during the start of the convalescent phase (>2 weeks after clinical symptom) and investigate the correlation among biological, and demographic factors. To increase the credibility of the comparative analyses, we first analyzed the plasma antibody levels, the golden standard to measure immune response to the viral infection. We then expanded to the mucosal antibody response and proteomic alterations at both systemic and mucosal levels.

Overall, our results demonstrate that saliva is not only a fluid for viral monitoring but also a reliable source in evaluating the immune responses in the short term and longitudinally. The immune dysfunctions found here are key determining protective and aberrant immune mechanisms at the mucosal level. The salivary proteome reflected such immunopathogenesis mediated by interactions among IgA, neutrophil, and fibrinogen, which was not observed in plasma proteome. Elevated fibrinogen appears to be an indicator of severity of inflammatory response in both systemic and mucosal responses. Our study reveals that immune dysfunction can be detected in saliva in persons who have recovered from COVID-19. Such biomarkers may be a good way to screen for PASC and may identify novel pathways and mechanisms that can be targeted therapeutically. In this report we further demonstrate that salivary IgA antibody responses to SARS-COV-2 could be involved in the neutrophil-fibrinogen interactions at the oral mucosal surface.

RESULTS

Salivary antibody patterns specific to the SARS-CoV-2 antigens were significantly correlated with matched plasma serology.

Paired plasma and salivary samples from COVID-19 donors in recovery phase (20-72 days) were collected and subjected to the comparative analyses among demographic factors (age, gender, and disease severity), antibody, and proteomic responses (**Fig. 1**) (**Suppl. Table. 1**). Samples collected from healthy individuals were included for comparison between health vs. COVID-19 (**Fig.1**). We first evaluated antibody response detected from saliva and plasma, specific for SARS-CoV-2 receptor binding domain (RBD), subunit 1 (S1) and subunit 2 (S2) of the spike protein, and the nucleoprotein (NP) (**Fig. 2A-C**). The antibodies to common cold coronaviruses were also evaluated by measuring the antibodies which bind to the NL63 (NL63) Spike pike Glycoprotein. Our primary interest was the antibodies specific to the RBD and S1 of SARS-CoV-2, the sites responsible for binding to cell receptors and major mutation sites. When comparing antibody titers in convalescent over healthy groups, significant increase was observed in RBD binding IgA in saliva ($p=0.0001$), RBD binding IgA in plasma ($p=0.0003$), S1 binding IgG in plasma ($p<0.0001$), and RBD binding IgM in saliva ($p=0.0118$) (**Fig. 2A-C**). Interestingly, significant correlations between paired saliva and plasma were also observed for the SARS-CoV-2 RBD or S1 binding immunoglobulins (**Fig. 2D**). Significant correlations among immunoglobulin subclasses in plasma and saliva were summarized in **Supplementary Table 2**.

Immunoglobulin composition and neutralizing functions presented unique patterns between saliva and plasma.

While the antibody response to the SARS-CoV-2 RBD and S1 showed significant correlation between saliva and plasma, the overall antibody profile of saliva was different than plasma. For

IgA response, convalescent saliva was significantly higher than convalescent plasma for SARS-CoV-2 S1, S2, NP, and NL63 ($p<0.0001$, $p=0.0036$ S1, $p=0.0009$ S2, and $p<0.0001$, respectively) (**Fig. 2A**). The IgG response showed an opposite trend in that the titers in convalescent plasma were significantly higher than convalescent saliva for SARS-CoV-2 RBD, S1, S2, and NP ($p=0.0178$, $p<0.0001$, $p<0.0001$, and $p<0.0001$) (**Fig. 2B**). The IgM response was also significantly higher in plasma than saliva for all four SARS-CoV and NL63 antigens ($p<0.0001$ for RBD, $p=0.0117$ for S1, $p<0.0001$ for S2, $p=0.0338$ for NP, and $p<0.0001$ for NL63).

When we evaluated the neutralizing activity against SARS-CoV-2 S bearing pseudovirus particles (rVSV-GFPΔG*Spike), saliva antibodies showed obviously lower neutralizing activity in comparison to plasma (**Suppl. Fig. 1**). Neutralizing activity in plasma samples was surprisingly higher than our expectation. Even though the donors in the healthy group never encountered the SARS-CoV-2 virus, more than half of their plasma displayed a significant level of neutralizing activity (62.5 %, median IC_{50}=271.10) to the pseudoviral particles. The convalescent donors showed increased neutralizing activity in plasma or both positive rate and titer (92.16%, median IC_{50}=317.30). In contrast, paired saliva samples were poor at the neutralizing activity despite the robust RBD-, and S1-binding IgA responses detected by ELISA (**Fig. 2A**). Only after purification and concentration of the IgAs in saliva[33], neutralizing activity was detected within a limited range from two COVID-19 salivary samples (16.22%, IC_{50}=10.00).

Immune dysfunction and chronic inflammatory pathways detection in global proteome analysis.

Saliva and plasma samples were further subjected to mass spectrometry and proteomic profiling's to provide a more comprehensive characterization of oral mucosal and systemic responses following SARS-CoV-2 infection. Dimension reduction by principal component analysis (PCA)

showed a separation of COVID-19 donors from healthy controls for both saliva and plasma samples (**Fig. 3A&B**). Differentially expressed (DE) proteins between convalescent over healthy samples were displayed as in volcano plots (**Fig. 3C&D**) and all significant observations were summarized in **Table 1**. The DE proteins, significantly enriched in convalescent saliva and plasma (fold change>2, p-value<0.05 in **Fig. 3C&D**), were presented as in bar graphs (**Fig. 3F&G**). There were no DE proteins significantly enriched in healthy over COVID-19 (fold change <-2, p-value<0.05 in **Fig. 3D&E**). In saliva, COVID-19 convalescent samples showed significant increase in expression of moesin (Uniprot accession number, AC=P26038, fold changes= 2.622, p-value<0.001), transmembrane protease serin D (AC=O60235,fold change=2.109, p-value=0.004), alpha-actin-1 (AC=P12814, fold changes= 2.450, p-value=0.004), nuclear transport factor 2 (AC=P61970, fold changes=2.251, p-value=0.0498), and serpin B13 (AC=Q9UIV8, fold changes= 2.293, p-value=0.001) (**Fig. 3C, E** and **Table. 1A**). The significantly enriched DEs in convalescent plasma in comparison to the healthy plasma were the fibrinogen alpha chain (AC=P0267, fold changes=3.279, p-value<0.001), Keratin, type II cytoskeletal 1 (AC=P04264, fold change=2.0231, p-value<0.001), apolipoprotein C-II (AC=P02655, fold changes=3.688, p=0.027), and REST corepressor2 (AC=Q8IZ40, fold changes=2.247, p-value=0.0122) (**Fig. 3D, F,** and **Table. 1B**).

The proteomic signature was further analyzed for the random forest machine learning and network analyses (STRING enrichment analyses). The hierarchical clustering heatmap generated from the random forest machine learning demonstrated the pathway is clustered into two groups based on COVID-19 vs. healthy (**Fig. 4A**). Network analyses performed based on differentially expressed proteins between COVID-19 and healthy samples (**Table 1**) showed that convalescent plasma proteome displayed suppressed biological functions involved in oxidative damage response, antimicrobial properties against opportunistic infection (*Staphylococcus aureus* infection) and complement and coagulation cascades (Plasma DOWN in **Fig. 4B**). In contrast, the

pathways enriched in COVID-19 plasma were all associated with the fibrin clot formation (Plasma UP in **Fig. 4B**). Pathways enriched in convalescent saliva samples included hemostasis, platelet degranulation, immune system, interleukin-12 signaling, and leukocyte activation (Saliva UP in **Fig. 4B**). The pathways related with the granule or lysozyme formation were suppressed in convalescent saliva (Saliva DOWN in **Fig. 4B**).

Altered proteomic functions in COVID19 convalescent saliva directly correlated with expression of RBD-binding IgA response in saliva.

Comparative proteomic analyses between healthy vs. COVID-19 suggests that inflammatory markers induced by COVID-19 remain in both plasma and saliva during the recovery phase (20-72 days from onset of clinical symptoms, average 45 days). For a better understanding of the inflammatory patterns occurring in the oral local mucosal and systemic immune system, we performed a separate set of analysis which compared the salivary and plasma proteome (**Fig. 5A**). The PCA analysis showed a clear separation between saliva and plasma proteome for both healthy and COVID-19 convalescent samples (**Fig.5B**). Hierarchical clustering heatmaps were clustered into two groups based on the origin of samples (saliva vs. plasma) while demographic factors (gender, age, and disease severity) did not contribute to the clustering. (**Fig. 5C&D**). In a healthy state, most DE proteins were higher in saliva, but proteins related to coagulation pathways (complement C3, C5, antithrombin) were observed higher in plasma (**Fig. 5C**). The COVID-19 heatmap was in a similar pattern with the healthy heatmap, except that the expression pattern of apolipoprotein and fibrinogen was reversed (saliva>plasma in healthy; plasma>saliva in COVID-19, **Fig. 5C&D**). The cluster of saliva in COVID-19 heatmap further diverged into three subclusters (Blue arrows and roman numerals on top of the **Fig. 5D**), suggesting the link between humoral immune response and innate inflammatory response at oral mucosa. Each cluster was labeled as I, II, and III in an increasing order of protein expression level.

Understanding the influence of the immune subclusters in relation to serological results within each fluid, we investigated the correlation with the immunoglobulin levels (**Fig.6A-C**). Strikingly, significant correlations were observed with the RBD-binding saliva IgA, IgM, and plasma IgA titers, as in a linear increase by the order of subcluster numbers (p=0.0274, p=0.0038, and p=0.0409, respectively, **Fig. 6A-C**). As we observed an increasing trend in the expression level of DE proteins among subclusters, we also performed correlation analysis between each RBD binding immunoglobulins with each DE protein involved in the COVID-19 saliva sub-clustering (**Fig. 6D-H**). The Clusterin (apolipoprotein J, uniprot accession number: P10909)[34] showed significant positive correlations with RBD binding IgA in saliva and plasma (**Fig. 6D&E**); fibrinogen beta chain was significantly correlated with RBD binding IgA in saliva (**Fig. 6F**); and Apolipoprotein A1 was correlated with the RBD binding salivary IgM and plasma IgA (**Fig. 6G&H**).

DISCUSSION

Collectively, we demonstrated that robust inflammatory responses to the SARS-CoV-2 remain in convalescent plasma and saliva despite the absence of clinical manifestation of PASC. Aberrant immune responses and blood clotting dysfunctions were detected in both saliva and plasma of COVID-19 cases. The biofluids investigated here demonstrated positivity for antibodies specific for SARS-CoV-2 receptor binding domain (RBD), subunit 1 (S1) and subunit 2 (S2) of the spike protein, and the nucleoprotein (NP). Clearly, significant increase was observed in RBD binding IgA in both saliva and plasma, S1 binding IgG in plasma, and RBD binding IgM in saliva. Significant correlations between paired saliva and plasma showed positivity for SARS-CoV-2 RBD or S1 binding immunoglobulins, showing that saliva is an available biofluid for monitoring the presence of protective antibody responses, and immune responses. Still, saliva displayed unique patterns unique patterns differentiated from plasma for both antibody and proteomic profiles. The IgA response in convalescence was significantly higher in saliva than plasma, whereas the IgG response showed an opposite trend in that the titers in convalescent plasma. This is expected as

IgG is the dominant subtype in blood[35]. While plasma only conveys the dysregulated blood clotting functions, saliva samples contained more information important to the immunopathogenesis, including dysregulated fibrin clot, dysregulated neutrophil pathways, potentially correlated with robust salivary IgA responses lacking in neutralizing activity. Thus, our initial findings open the perspective of saliva as a viable immune biofluid. Saliva is easy to collect and does require a specialty clinic or phlebotomist professional, and special containment to be applied for early diagnosis and prevention of virus-induced chronic inflammatory sequelae.

When evaluating the biofluids via shot-gun proteomics, we aimed to understand how these immunoglobulin patterns found in COVID-19 would impact the composition and function of the entire repertoire of human proteins, thus investigating molecular patterns, early events that drive signals before disease manifests. The plasma proteomics of COVID-19 samples revealed dysregulated blood clot process, and salivary proteomics showed more responses related to the innate immune compartment. We found that salivary moesin, alpha-actinin-1 and nuclear transport factor 2 are involved in migration of neutrophils [36–38]. And serpin B13 is known to regulate neutrophil serine proteases and inflammatory caspases [39]. If not limited to the proteins upregulated by 2 fold or higher, convalescent saliva showed increase in numerous proteins associated with neutrophil functions or migration, such as Annexin 1[40,41], antileukoproteinase[42], and Matrix metalloproteinase-9[43,44] (**Table 1A**). At the same time, the convalescent saliva showed significant increase in transmembrane protease serine 11D, which is known to activate the SARS-CoV-2 spike protein and facilitate the viral-cell fusion process[45,46]. It warrants that neutrophil-driven innate immune response at oral mucosa initiates a dysbiotic cycle, tissue damage that ultimately leads to prolonged infection-inflammation sequelae. In severe COVID-19 cases, neutrophil degradation and NETosis in blood and lung have been functionally linked to severe inflammation and thrombosis [14,15,47–50]. These molecular consequences of COVID-19 are now well studied. In a condition termed post-acute sequelae SARS-CoV-2 infection (PACS) or long COVID

[51–53], patients have chronic inflammatory disease over multiple organs. But here, we show molecular consequences of COVID-19, clearly emphasizing molecular dysfunctions leading to chronic inflammation.

In addition to chronic dysfunction detected, abnormal fibrinolysis is known to impact networks with neutrophil functions, including NETs (Neutrophil Extracellular Traps)[48,54,55]. In fact, excessive release of NETs, with low resolution of inflammation, can lead to immune thrombosis within blood vessels, and the NET-fibrin interactions can contribute to the severity of tissue injury and pathogenesis [56]. Unique to the oral organ, the NETs-fibrin axis plays a unique role to regulate constant deposition of fibrin produced by the commensal-triggered inflammation[57]. Our proteomic analyses also revealed significant correlations between salivary fibrinogen and salivary annexin-1. More strikingly, our comprehensive analysis further demonstrated the potential role of salivary IgA response in the NET-fibrin interaction. The plasma fibrinogen alpha chain displayed significant correlation with salivary markers, such as salivary RBD IgA and salivary IgM (**Table 2**). Significant correlations were also observed between the salivary RBD IgM and salivary RBD IgA; salivary RBD IgM and salivary fibrinogen beta chain; salivary RBD IgM and categorized disease severity. It suggests that salivary antibodies to the SARS-CoV-2 infection participate in the inflammatory response mediated via NET-fibrin in oral mucosa and possibly contribute to the systemic inflammatory response represented by enhanced plasma fibrinogen.

The potential for IgA to promote proinflammatory response by innate immune cells has been reported for both health and disease models. Aleyd et al[58] demonstrated that IgA enhances NETosis as an effective defense mechanism to eliminate pathogens at mucosal surfaces. In contrast, neutrophil activation by IgA immune complex is also known to contribute to the immunopathogenesis of autoimmune diseases, such as IgA vasculitis, nephropathy [59–61]. In respiratory viral disease models, such as influenza and SARS-CoV-2, formation of an IgA-virus

immune complex led to exacerbated NETosis[62]. Because our samples mimic the physiological composition (whole saliva, whole plasma), we began to isolate our molecules to understand their specific functions versus binding and detection.

Neutralizing activity detected from plasma samples is expected to reduce the chance of severe illness from SARS-CoV-2 infection[63]. We detected robust IgA response in saliva to the SARS-CoV-2 infection, with limited range of neutralizing activity. The secretory IgA, predominantly dimeric form, confers superior neutralizing activity at respiratory mucosal lining against SARS-CoV-2, and influenza viruses [64–66]. A recent study demonstrated that neutralizing activity of salivary IgA induced by SARS-CoV-2 infection was maintained up to 73 days after clinical symptom, but later time points (189-230 days) [67]. Salivary IgAs induced by vaccination with BNT162b2 showed similar kinetics in that the binding activity specific to the SARS-CoV-2 RBD peaked at 85-120 days post vaccination but diminished by 170-205 days[68]. Both studies demonstrated that the salivary IgAs secreted as in polymeric form (dimeric and tetrameric) were superior to confer neutralizing activity than IgGs. Underlying mechanism of poor neutralizing activity of salivary IgA, observed in this study, will be essential to understand the reinfection of the SARS-CoV-2 and devise prophylactic strategy. Saliva is an important vehicle for the spread of the SARS-CoV-2 viruses and a critical target to end the explosive transmission of the SARS-CoV-2 viruses[69,70]. It was not the primary goal of our study to understand the full biology of neutralizing antibodies in saliva, but rather investigate detection and the immune pathology of convalescent donors. Yet, oral mucosal compartment provides direct protection against infection or prevention of disease and leveraging these natural findings can lead to better understanding of host-viral interacts in several stages of the cycle of the virus. The ability to activate a robust mucosal antiviral response should be further investigated in the development of future preventive measures, including vaccines.

Limitation of our study consists of selection bias of donors enrolled in our study with inclusion criteria that considered most donors that had SARS-CoV-2 RT-qPCR-positive results and not healthy donors. The control population came from a pre-COVID era, and did not include an RT-qPCR, but attempted to match most of the demographics. Since our analysis was based on convalescent samples passively collected from persons with COVID-19 in the recovery phase, our study result does not directly reflect responses during the active disease phase of the viral infection. Some parameters, such as RBD binding IgG responses, seem to be already waned and did not display significant differences from healthy. While we could detect unresolved inflammatory status lagged from the acute phase of COVID-19, our study setting was not optimal to elucidate innate immunopathogenesis. As our data set was missing critical information, such as viral load, we cannot fully exclude the confounding factors that could possibly impact the antibody and proteomic alterations. Also, the samples were collected at only a one-time point, and antibody levels or proteomic responses were not adjusted by the different baseline of each individual and it was not possible to draw predictive conclusions on our findings but instead correlations. Most importantly, this is our cross-sectional study investigating one time point comparing health vesus disease and saliva versus plasma.Future longitudinal studies should investigate mechanistically of how inflammatory profile is stablished and understand the transition from the onset of clinical sequel tp PACS. Clearly this would lead to identification of predisposing factors and the ultimately understanding of disease pathogenesis.

Overall, early dysfunctional immune responses and blood clotting pathway dyscrasias are detected in saliva and plasma of COVID-19 cases. Saliva is an important vehicle for the spread of the SARS-CoV-2 viruses and a fluid for detection of not just antibody responses, but also diverse immune pathways, including mucosal immunity, innate immune responses, neutrophil functions, and others. Comparative analysis of the antibody and proteomic profile suggests the

distinct signatures in local oral mucosa when compared to systemic immune responses. Convalescent plasma samples exhibited IgG-centered antibody profiles with high neutralizing potency plus dysregulation in blood clotting factors in comparison to healthy samples. Saliva showed higher concentration of IgA response with lower neutralizing activity, but with activation of novel immune markers related to disease development. Here, we highlight that our participants did not completely resolve from the SARS-CoV-2 infections, which in turn led to chronic inflammation and blood clotting dysfunctions, without clear clinical manifestations during the convalescent phase. The potential of saliva to dissect immunopathogenesis in the context of population analysis can offer better understanding of the mucosal and innate immune response kinetics and specificity to exposure to SARS-CoV-2 and various infectious agents.

METHODS

The research reported in this manuscript complies with all relevant ethical regulations and informed consent was obtained from all human participants. Additional information was collected on donor demographics (age and gender).

Ethic Approval

This study has been approved by the University of California, San Diego Institutional Review Board (IRB, no. 200236X) and the J. Craig Venter Institute (IRB, no. 2020-286).

Experimental study design

Blood and saliva samples were collected from COVID-19 donors who visited the COVID clinic in the University of California, San Diego (n=34). Confirmed COVID-19 cases were defined as previously described [71]. Throughout the sample collection, the major SARS-CoV-2 strain circulating throughout the study was the original strain (USA-WA1/2020) and the vaccine against SARS-CoV-2 was not available. For comparison, we included healthy donors (n=13) from pre-

pandemic era and recruited to this study signed the institutional review board (IRB)– approved consent form (# 2018-268) [72].

Peripheral blood samples collected by venipuncture and collected into BD vacutainer SST tubes (Vitality Medical, Salt Lake City, Utah). After 1hr., the collected blood sample was centrifuged for serum separation. Saliva was collected by the “passive drool technique” using the Saliva Collection Aid (Salimetrics, Carlsbad, CA). All samples were aliquoted and stored at −80°C for long-term storage.

General experimental approach was summarized in Figure 1. Briefly, all collected plasma and saliva samples were tested for SARS-CoV-2 specific antibodies by enzyme-linked immunosorbent assay (ELISA) and pseudovirus neutralization assay (**Fig. 2 and Suppl. Fig. 1,** respectively). Correlations among all immunoglobulins (Ig) were investigated with Pearson’s correlation and simple linear regression analysis using the GraphPad Prism version 8.3.1. In parallel, separate sets of samples were processed and used for mass spectrometry to detect host antiviral-, and microbial proteins and peptides (**Fig 3-5**). At the end, all collected data was collectively analyzed to verify the interaction among systemic and oral mucosal immune response to the SARS-CoV-2 infection (**Fig. 6)**.

Antibody responses

SARS-CoV-2 binding ELISAs Plasma and saliva samples were tested for binding to recombinant SARS-CoV-2 using an Enzyme-linked immunosorbent assay (ELISA) according to the manufacturers with slight modifications. The recombinant spike protein from human coronavirus NL63 (NL63) was also included as a coating antigen to estimate the presence of cross-reactive antibodies to common cold coronaviruses. All procedure was repeated twice, once manually and once by using Hamilton Microlab STAR (Hamilton, Reno, NV). Briefly, ELISA plates (Nunc MaxiSorp™ flat-bottom, Thermo Fisher Scientific, Waltham, MA) were coated with antigen

(10ng/50μL) at 4 °C overnight. The binding site on the SARS-CoV-2 and detect cross-reactivity to human coronavirus NL63 (HCoV-NL63), four different coating antigens were included; SARS-CoV-2 Spike Glycoprotein (S1) RBD, His-Tag (HEK293)(NativeAntigen, Oxfordshore, United Kingdom), SARS-CoV-2 Spike Glycoprotein (S1), His-Tag (Insect Cells) (NativeAntigen, Oxfordshore, United Kingdom), SARS-CoV-2 Spike Glycoprotein (S2), His-Tag (Insect Cells) (NativeAntigen, Oxfordshore, United Kingdom), SARS-CoV-2 Nucleoprotein, His-Tag (E. coli) (NativeAntigen, Oxfordshore, United Kingdom), and Human Coronavirus NL63 Spike Glycoprotein (S1) His-Tag (HEK293) (NativeAntigen, Oxfordshore, United Kingdom). Next day, coated plates were washed three times with PBS-Tween (0.05%) and blocked with 200 μl of 5% milk blocking solution at room temperature for 30 min. During incubation, plasma and saliva samples were initially diluted 1:54 and 1:2, respectively, and three-fold serial dilution was performed. After blocking, diluted samples were added to the wells (50 μL/well) and incubated for 1 hr at room temperature. After 4X washing, 100 μL of 1:5000 diluted Goat anti-human secondary antibody was added into each well and incubated at 37°C for 1 hr (Goat Anti-Human IgG ɣ Chain Specific HRP conjugated, species Adsorbed (Human IgM, IgD and IgA) Polyclonal Antibody for IgG (Cat# AP504P, EMD Millipore, Burlington, MA), Goat Anti-Human IgA, a-chain specific Peroxidase conjugate for IgA (Cat# 401132-2ML, Calbiochem, San Diego, CA) for IgA, and Goat Anti-Human IgM Fc5μ Fragment specific HRP conjugated secondary antibody for IgM (Cat# AP114P, EMD Millipore, Burlington, MA). After the incubation, plates were washed four times and 200 μL of substrate (cat# P9187, Sigma, St. Louis, MO) was added for color development. After incubation in a dark room for 20 minutes, the reaction was stopped by addition of 50 μL 3M H2SO4 and plates were read at 450 nm. Positive response was determined by the area under the curve (AUC) using GraphPad Prism version 8.3.1 (GraphPad Software, Inc., San Diego, CA, USA).

Generation of pseudo-virus (rVSV-GFPΔG*Spike)

For pseudoviruses construction, spike genes from strain Wuhan-Hu-1 (GenBank: MN908947) were codon-optimized for human cells and cloned into eukaryotic expression plasmid pCAGGS to generate the envelope recombinant plasmids pCAGGS.S as described previously with slight modifications [73]. For this VSV pseudovirus system, the backbone was provided by VSV G pseudotyped virus (G*ΔG-VSV) that packages expression cassettes for firefly luciferase instead of VSV-G in the VSV genome. Briefly, 293T cells were transfected with pCAGGS.S (30 μg for a T75 flask) using Lipofectamine 3000 (Invitrogen, L3000015) following the manufacturer's instruction. Twenty-four hours later, the transfected cells were infected with G*ΔG-VSV with a multiplicity of four. Two hours after infection, cells were washed with PBS three times, and then a new complete culture medium was added. Twenty-four hours post infection, SARS-CoV-2 pseudoviruses containing culture supernatants were harvested, filtered (0.45-μm pore size, Millipore, SLHP033RB) and stored at −70°C in 2-ml aliquots until use. The 50% tissue culture infectious dose (TCID50) of SARS-CoV-2 pseudovirus was determined using a single-use aliquot from the pseudovirus bank; all stocks were used only once to avoid inconsistencies that could have resulted from repeated freezing-thawing cycles. For titration of the SARS-CoV-2 pseudovirus, a 2-fold initial dilution was made in hexaplicate wells of 96-well culture plates followed by serial 3-fold dilutions (nine dilutions in total). The last column served as the cell control without the addition of pseudovirus. Then, the 96-well plates were seeded with trypsin-treated mammalian cells adjusted to a pre-defined concentration. After 24 h incubation in a 5% CO2 environment at 37°C, the culture supernatant was aspirated gently to leave 100 μl in each well; then, 100 μl of luciferase substrate (Perkinelmer, 6066769) was added to each well. Two min after incubation at room temperature, 150 μl of lysate was transferred to white solid 96-well plates for the detection of luminescence using a microplate luminometer (PerkinElmer, Ensight). The positive well was determined as ten-fold relative luminescence unit (RLU) values higher than the

cell background. The 50% tissue culture infectious dose (TCID50) was calculated using the Reed–Muench method, as described previously [74].

Pseudovirus neutralization assay

Neutralizing activity against rVSV-GFPΔG*Spike was determined as previously described with slight modification [75]. Briefly, Vero cells were seeded at a density of 2.5 X 10^4/50 µL in a Greiner Bio-One™ CellStar™ µClear™ 96-Well, Cell Culture-Treated, Flat-Bottom, Half-Area Microplate (Thermo Fisher Scientific, Waltham, MA). Next day, the cell monolayer was rinsed with 0.01M PBS (Thermo Fisher Scientific, Waltham, MA). Due to the contamination by the commensal bacteria in saliva, total IgA was purified from saliva using Peptide M/agarose (InvivoGen Inc., San Diego, CA, USA) and used for the neutralization at low-dilution (1:2-1:10), as previously described[33]. Plasma and saliva IgAs were three-fold diluted (starting from 1:50 and 1:2 dilution, respectively) with infection media (DMEM medium (cat# 11995065, Thermo Fisher Scientific, Waltham, MA) containing 2% fetal bovine serum (FBS)). Twenty-five µL of diluted samples was incubated with the same volume of pseudovirus (rVSV-GFPΔG*Spike) at 37°C for one hr. The sample-virus mixture was added onto the Vero Cell monolayer and incubated at 37°C with 5% CO_2. On the following day (12~16 hrs.), the expression of GFP was visualized and quantified by Celigo Image Cytometer (Cyntellect Inc, San Diego, CA). The neutralizing activity of the plasma sample was determined as pNT_{50} calculated from a transformed non-linear regression curve generated by GraphPad Prism version 8.3.1. (GraphPad Software, Inc., San Diego, CA, USA). Due to low titer of salivary samples, the 50% inhibitory dilution (IC_{50}) was determined by the reciprocal of highest dilution of sample corresponding to 50% reduction in GFP count compared with virus control minus sample control using the Reed-Muench method [76] .

Proteomics and peptidomics sample preparation

Deactivated saliva and plasma specimens were first passed through 10-kDa cutoff filters (Microcon, Millipore). The filtrates and the remaining materials on filters were subjected to peptidomics and proteomics analysis, respectively. For peptidomics analysis, the filtrates were dried in SpeedVac, and resuspended in 20 ul LC buffer A (0.1% formic acid in water). For proteomics analysis, the proteins remaining on filters were digested using filter aided sample preparation (FASP) approach as described previously [77].

Liquid Chromatography with tandem mass spectrometry (LC-MS/MS) analysis.

For the LC-MS/MS analysis, the Ultimate 3000 nanoLC coupled to Q Exactive mass spectrometer (Thermo Scientific) was used. Peptides were first loaded onto a trap column (PepMap C18, 2 cm x 100 mm x I.D.; Thermo Scientific), and they were separated using in-house packed analytical column (C18 ReproSil, 3.0 mm, Dr. Maisch GmbH; 20 cm x 75 mm I.D.) and binary buffer system (buffer A: 0.1% formic acid in water; buffer B: 0.1% formic acid in acetonitrile) with a 150-min gradient (2-35% buffer B over 105min; 35-80% buffer B over 10min; back to 2% B in 5 min for equilibration after staying on 80% B for 5 min). For the MS data acquisition, a top-10 data-dependent acquisition (DDA) method was applied. The maximum injection time was set to 20 ms, and the scan range was set to 350–1800 m/z with an AGC target of 1e6. The MS/MS acquisition was performed with 30% HCD collision energy. The target value was set to 5e5, and maximum injection time was set to 100ms. Full MS and MS/MS scans were acquired at resolution of 70,000 and 17,500, Respectively. Dynamic exclusion was set to 20s. The mass to charge ratio (m/z [Da]) from mass spectrometry data was normalized and used for calculation of fold changes of differentially expressed (DE) proteins (health vs. COVID-19; saliva vs. plasma).

Database Search and Bioinformatics Analysis

For proteomics data analysis, protein identification and quantitation were performed using the MaxQuant-Andromeda software suite (version 1.6.3.4) as previously described [78]. Majority of the default settings were taken, including trypsin as enzyme, two missed cleavage sites, peptide length with minimum seven amino acids, oxidation (M) as variable modification and carbamidomethylation (C) as fixed modification. An UniProt human sequence database (20,376 sequences) was used for protein database search. False discovery rate (FDR) was set at 1% on both protein and peptide levels. Significantly enriched proteins in convalescent samples ($p<0.05$)(**Table 2**) were subjected to the network analysis by STRING enrichment analysis (Cytoscape software v. 3.9.1) [79]. The heatmap was created using the pheatmap package in R using hierarchical distance matrix and clustering option [80]. The volcano plots were generated using the EnhancedVolcano package in R [80].

Statistics

Data was statistically analyzed using the R or Graphpad Prism-8 suites of software (GraphPad Software, Inc., San Diego, CA, USA). Representatives of a minimum of two independent experiments were presented as the median and standard deviation and are representative of a minimum of two independent experiments. Data points for quantitative *in vitro* experiments represent all technical repeats for experiments done in triplicate. Antibody titers were analyzed by mixed-effect analysis with Tukey's multiple comparisons. Significance of fold changes in DE proteins were measured using the Student's t-test. Correlation among different parameters (antibody titers, proteomic marker expression levels, categorized demographic information, and salivary protein subgrouping) was evaluated by both Pearson's R and simple linear regression analyses using Graphpad Prism-8 suites of software (GraphPad Software, Inc., San Diego, CA, USA).

Data Availability

The raw proteomic data that support the findings of this study are shown in the source data file (ftp://MSV000086946@massive.ucsd.edu) at the Global Natural Products Social (GNPS) molecular networking depository via the Mass spectrometry Interactive Virtual Environment (MASSIVE) [81].

Code Availability

Current study did not use custom code or mathematical algorithms. All code or mathematical methods used for analyses were described above.

Acknowledgements

We would like to thank Wan Choi for technical support. This work was supported in part by The Conrad Prebys Foundation Grant (20-122), U.S. Public Health Service Grants (R00 DE0234804) from the National Institute of Dental and Cranial Research (given to MF).

Author contributions

The authors confirm contribution to the paper as follows, study conception and design: Marcelo Freire; sample collection: Davey Smith, Stephen A. Rawlings; data collection: Marcelo Freire, Gene S. Tan, Yanbao Yu, Benjamin L. Sievers, Terri Gelbart, Harinder Singh, Hyesun Jang; analysis and interpretation of results: Marcelo Freire, Hyesun Jang, Gene S. Tan, Yanbao Yu, Harinder Singh; draft manuscript preparation: Hyesun Jang, Marcelo Freire, and Harinder Singh. All authors reviewed the results and approved the final version of the manuscript.

Competing interests

Dr. Davey Smith DMS has consulted for FluxErgy Inc, Kiadis Pharmaceuticals, Bayer Pharmaceuticals, Linear Therapies, Matrix Biomed, Model Medicines, VxBiosciences, and Brio Clinical. Dr. Marcelo Freire has consulted for Mars Wrigley.

ORCID for corresponding authors

Marcelo Freire 0000-0003-4906-7698

FIGURE LEGENDS

Figure 1. Study Design.

Serum and plasma samples were collected from healthy (n=13) and coronavirus disease (COVID-19) donors (n=34) to investigate the viral-immune axis in health versus disease. Along with the demographic factors, the plasma and saliva samples were tested for the antibody response and shotgun proteomics followed by network, pathway, and correlation analyses. This study was designed to capture the inflammatory response during the start of the convalescent phase (>2 weeks after clinical symptom). Ultimately, our findings will be applied to discover early detection markers for the post-acute sequelae of SARS-CoV-1 infection. *EHR= Electronic Health Record*

Figure 2. Compartmentalized antibody response found in saliva and plasma collaborate in response to the SARS-CoV-2 infection.

(A-C) The individual area under the curve (AUC) of enzyme-linked immunosorbent assay (ELISA) titers was plotted as blue circles (saliva) or red triangles (plasma). Bars and whiskers represent median and standard deviation, respectively. Mixed-effect analysis with Tukey's multiple comparisons test was used to measure statistical significance. *$*p \leq 0.05$; $**p \leq 0.01$; $***p \leq 0.001$; $****p \leq 0.0001$*. **(D)** Four paired immunoglobulins showing significant correlation ($p<0.05$) between plasma and saliva were depicted as simple linear regression models. The individual titer of saliva

was plotted by paired plasma titers. Predicted regression line and deviations were depicted as solid and dotted line, respectively. Functions and p-value of regression analyses were indicated next to the regression lines. Correlations of immunoglobulins specific to the SARS-CoV-2 receptor binding site (RBD) or Spike protein 1 (S1) were colored yellow and red, respectively.

Figure 3. Comparative proteomic analyses revealed differentially expressed proteins (DEs) enriched by the SARS-CoV-2 infection for both saliva and plasma.

(A&B) Dimension reduction by principal component analysis (PCA) showed a separation of proteins from COVID-19 donors from healthy controls in saliva and plasma, respectively. Circles indicate 95% confidence intervals of group memberships. Percentages along the axes indicate the degree of variance explained by that principal component. **(C&D)** Fold changes of protein expression of COVID-19 over healthy samples were plotted by negative log-transformed p-values in volcano plots. Dotted lines of volcano plot represent thresholds for the Log2 fold changes and statistical significance (±1 and $p<0.05$, respectively). **(E&F)** Relative abundance of differentially expressed proteins (Log2 fold changes>1, $p<0.05$) in saliva and plasma, were depicted as in box and whiskers plots. Individual dots represent individual values. Interquartile range, median, and min/max values were illustrated as box, middle line and whiskers, respectively. Mixed-effect analysis with Tukey's multiple comparisons test was used to measure statistical significance. *$*p \leq 0.05$; $**p \leq 0.01$; $***p \leq 0.001$; $****p \leq 0.0001$. DE=differentially expressed proteins*

Figure 4. Network analyses depicted altered pathways and functions in convalescent plasma and saliva.

(A) Significantly enriched differentially expressed (DE) proteins in COVID-19 vs. Healthy individuals were subjected to the random forest machine learning and proteins that showed 100% accuracy predicted were plotted in the heatmap. Dendrogram was constructed based on hierarchical clustering and the group information (healthy vs. COVID-19) was color coded. **(B)** In

parallel, interactions among DE proteins were predicted by the STRING enrichment analyses and depicted as network maps. Pathways associated with each DE protein was depicted as in a donut graph, color-coded based on terms discovered by STRING enrichment assay.

Figure 5. Comparative proteomic analyses showed heterologous signatures of each biofluid and cues to immune pathology.

(A) The proteomics data was further analyzed to compare proteomic composition between saliva vs. plasma. The data obtained from healthy and COVID-19 participants was separately analyzed. (**B)** Differentially expressed proteins (Log2 fold changes>1, $p<0.05$) in saliva and plasma, were depicted as in relative abundance of five significantly up-regulated proteins. The 95% confidence intervals of group memberships and degree of variance was indicated as circle and percentages on the axes, respectively. **(C&D)** The heterologous proteomic profile between saliva and plasma was further analyzed using clustered heatmap for both healthy and COVID-19. Relative abundance was calculated based on the proportion of normalized reads and displayed as color gradients. Dendrogram was constructed based on hierarchical clustering of relative abundances and color-coded demographic information of each participant was added to show their association with each clade. Blue Roman numerals and arrows indicate subclades in COVID-19 saliva. The numbering was in crescent with the expression level of DE proteins.

Figure 6. Correlation analysis suggests that proteomic alterations in convalescent saliva is associated with antibody responses specific to the receptor binding site (RBD) of SARS-CoV-2.

(A-C) Significant correlation ($p<0.05$) between SARS-CoV-2 RBD specific immunoglobulins and COVID-19 salivary sub-clusters were depicted as simple linear regression models. The individual titer of immunoglobulin was plotted by subcluster numbers. Predicted regression line and deviations were depicted as solid and dotted line, respectively. Functions and p-value of

regression analyses were indicated next to the regression lines. **(D-H)** Three differentially expressed proteins responsible for the clustering were illustrated as simple regression models as described above

Supplementary figure 1. Pseudovirus neutralization by plasma and saliva samples.

Neutralizing potency of plasma and saliva sample was measured by neutralizing activity to VSV pseudoviruses bearing S protein (rVSV-GFPΔG*Spike). Percentage of plasma or saliva samples with neutralizing activity was depicted as in pie chart **(A)**. Representative images of inhibition of GFP expression by saliva samples were displayed in **(B)**.

FIGURES

Figure 1. Study design

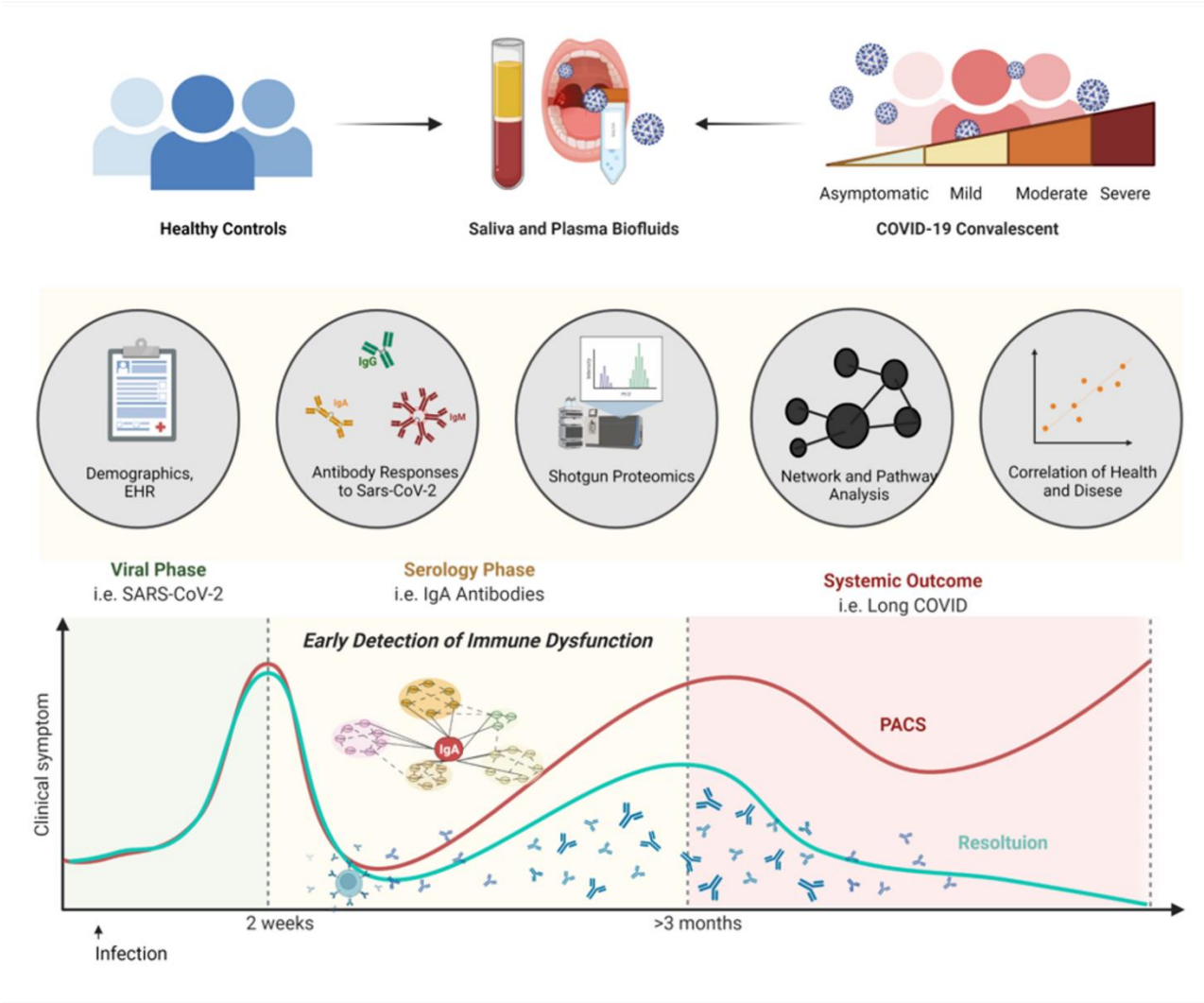

Figure 2. Compartmentalized antibody response found in saliva and plasma collaborate in response to the SARS-CoV-2 infection.

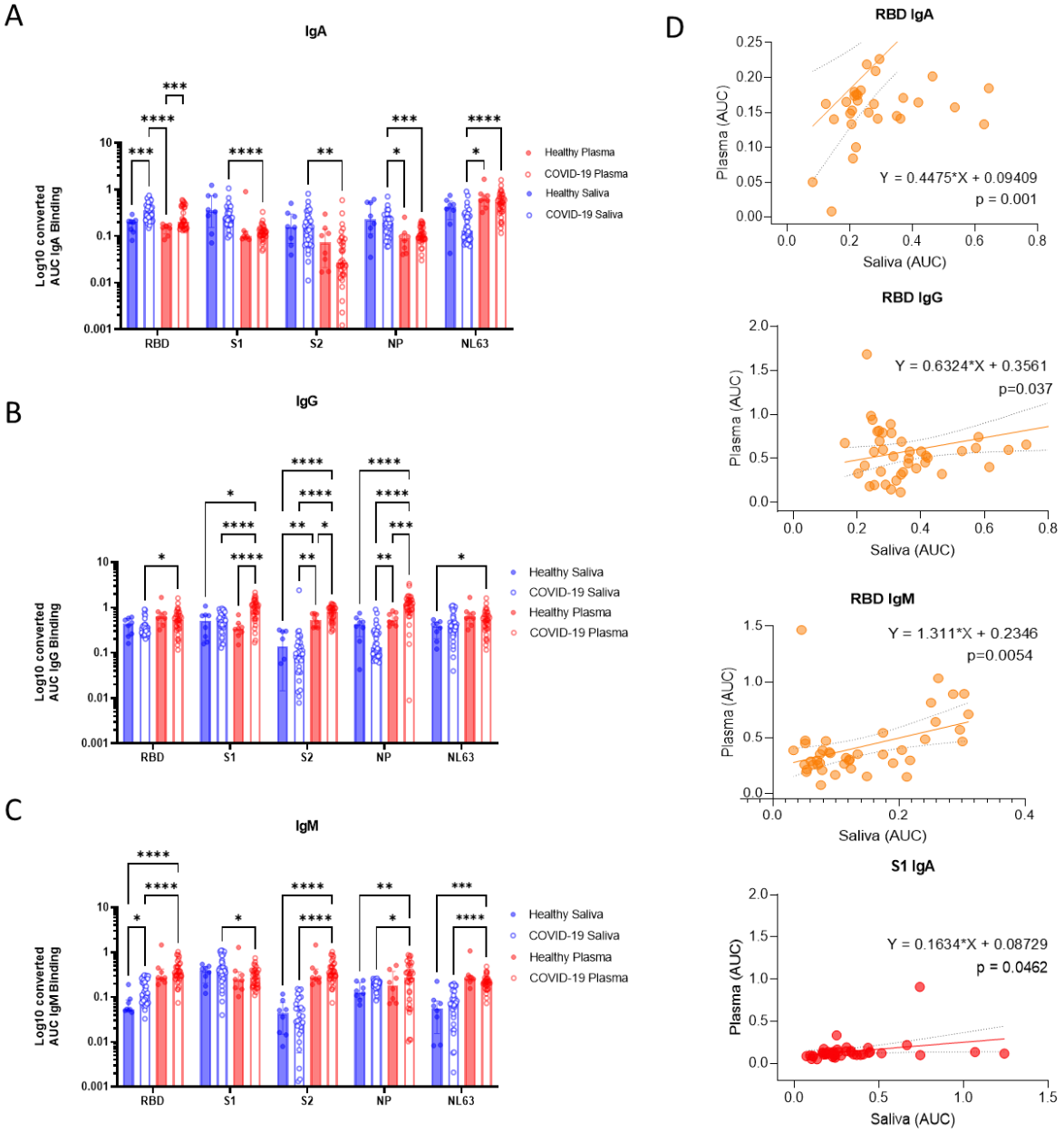

Figure 3. Comparative proteomic analyses revealed differentially expressed proteins (DEs) enriched by the SARS-CoV-2 infection for both saliva and plasma.

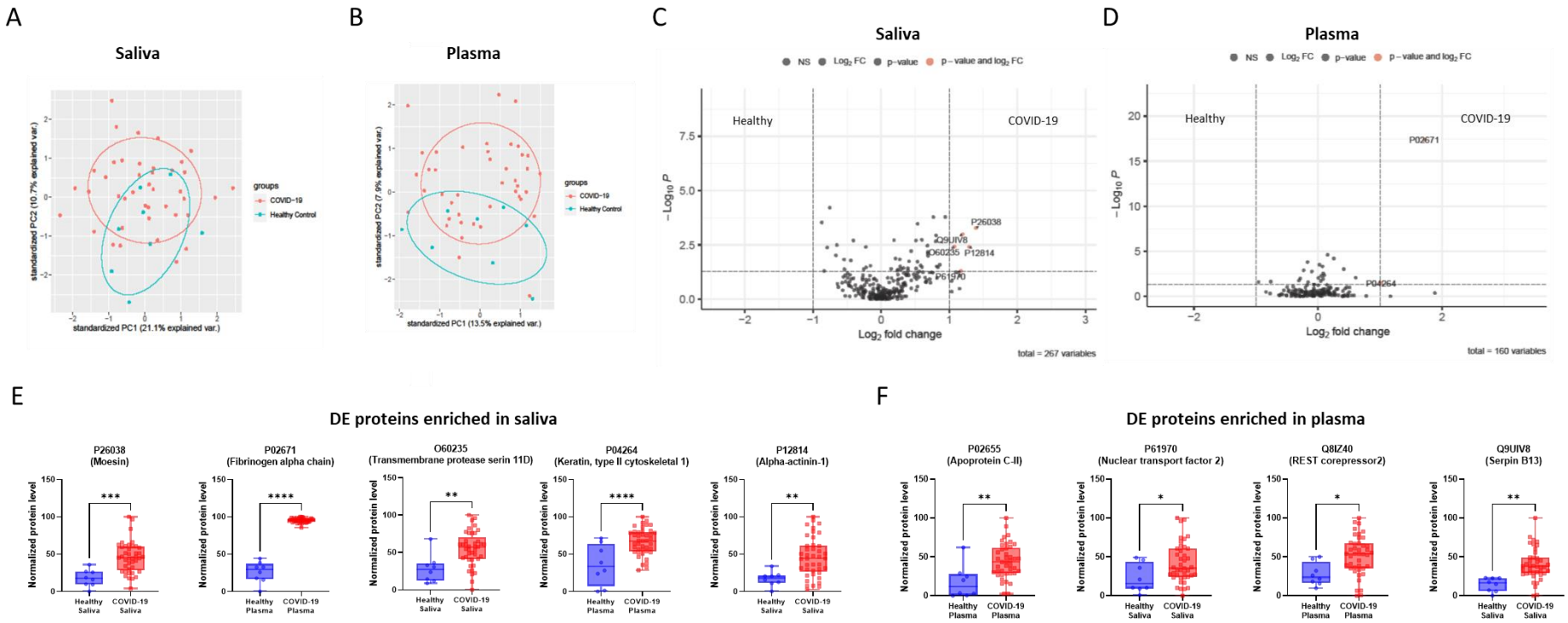

Table 1. Significant observations (p<0.05) in fold changes of differentially expressed proteins in the saliva of COVID-19 and healthy samples.

A. Saliva

Uniprot code (AC)	Healthy Median	COVID-19 Median	Fold changes (COVID-19/ Healthy)	P-value	Function
P02655	11.8027	43.5327	3.6884	0.0027	Apolipoprotein C-II (Apo-CII) (ApoC-II) (Apolipoprotein C2) [Cleaved into: Proapolipoprotein C-II (ProapoC-II)]
P02671	29.1875	95.7101	3.2791	0.0000	Fibrinogen alpha chain [Cleaved into: Fibrinopeptide A; Fibrinogen alpha chain]
Q8IZ40	23.9837	53.8844	2.2467	0.0122	REST corepressor 2
P04264	33.4788	67.7300	2.0231	0.0001	Keratin, type II cytoskeletal 1 (67 kDa cytokeratin) (Cytokeratin-1) (CK-1) (Hair alpha protein) (Keratin-1) (K1) (Type-II keratin Kb1)
P01594	30.1460	51.6788	1.7143	0.0414	Immunoglobulin kappa variable 1-33 (Ig kappa chain V-I region AU) (Ig kappa chain V-I region Ka)
P00734	33.2410	49.7230	1.4958	0.0150	Prothrombin (EC 3.4.21.5) (Coagulation factor II) [Cleaved into: Activation peptide fragment 1; Activation peptide fragment 2; Thrombin light chain; Thrombin heavy chain]
P00748	33.0656	46.1847	1.3968	0.0390	Coagulation factor XII (EC 3.4.21.38) (Hageman factor) (HAF) [Cleaved into: Coagulation factor XIIa heavy chain; Beta-factor XIIa part 1; Coagulation factor XIIa light chain (Beta-factor XIIa part 2)]
P08697	36.4384	50.8219	1.3947	0.0279	Alpha-2-antiplasmin (Alpha-2-AP) (Alpha-2-plasmin inhibitor) (Alpha-2-PI) (Serpin F2)
Q9UBP9	57.9882	77.2189	1.3316	0.0009	PTB domain-containing engulfment adapter protein 1 (Cell death protein 6 homolog) (PTB domain adapter protein CED-6) (Protein GULP)
Q5T5C0	71.3590	85.0463	1.1918	0.0153	Syntaxin-binding protein 5 (Lethal(2) giant larvae protein homolog 3) (Tomosyn-1)
P09871	87.7720	78.0244	0.8889	0.0413	Complement C1s subcomponent (EC 3.4.21.42) (C1 esterase) (Complement component 1 subcomponent s) [Cleaved into: Complement C1s subcomponent heavy chain; Complement C1s subcomponent light chain]
P02743	85.6530	70.3051	0.8208	0.0024	Serum amyloid P-component (SAP) (9.5S alpha-1-glycoprotein) [Cleaved into: Serum amyloid P-component(1-203)]
A0A0B4J1X5	77.7429	60.2926	0.7755	0.0233	Immunoglobulin heavy variable 3-74
P01871	43.7500	33.1422	0.7575	0.0397	Immunoglobulin heavy constant mu (Ig mu chain C region) (Ig mu chain C region BOT) (Ig mu chain C region GAL) (Ig mu chain C region OU)
P27169	60.6238	45.7115	0.7540	0.0226	Serum paraoxonase/arylesterase 1 (PON 1) (EC 3.1.1.2) (EC 3.1.1.81) (EC 3.1.8.1) (Aromatic esterase 1) (A-esterase 1) (K-45) (Serum aryldialkylphosphatase 1)
P01591	65.5666	49.2849	0.7517	0.0054	Immunoglobulin J chain (Joining chain of multimeric IgA and IgM)
P01011	57.4541	42.7752	0.7445	0.0442	Alpha-1-antichymotrypsin (ACT) (Cell growth-inhibiting gene 24/25 protein) (Serpin A3) [Cleaved into: Alpha-1-antichymotrypsin His-Pro-less]
P00738	81.8642	60.6936	0.7414	0.0209	Haptoglobin (Zonulin) [Cleaved into: Haptoglobin alpha chain; Haptoglobin beta chain]
P06276	60.0000	43.2934	0.7216	0.0014	Cholinesterase (EC 3.1.1.8) (Acylcholine acylhydrolase) (Butyrylcholine esterase) (Choline esterase II) (Pseudocholinesterase)

P0C0L5	61.3569	44.1003	0.7187	0.0061	Complement C4-B (Basic complement C4) (C3 and PZP-like alpha-2-macroglobulin domain-containing protein 3) [Cleaved into: Complement C4 beta chain; Complement C4-B alpha chain; C4a anaphylatoxin; C4b-B; C4d-B; Complement C4 gamma chain]
P80108	83.2759	58.6207	0.7039	0.0144	Phosphatidylinositol-glycan-specific phospholipase D (PI-G PLD) (EC 3.1.4.50) (Glycoprotein phospholipase D) (Glycosyl-phosphatidylinositol-specific phospholipase D) (GPI-PLD) (GPI-specific phospholipase D)
P02747	63.9785	43.6559	0.6824	0.0159	Complement C1q subcomponent subunit C
P36955	87.1739	58.6232	0.6725	0.0007	Pigment epithelium-derived factor (PEDF) (Cell proliferation-inducing gene 35 protein) (EPC-1) (Serpin F1)
P00736	85.4198	56.7176	0.6640	0.0141	Complement C1r subcomponent (EC 3.4.21.41) (Complement component 1 subcomponent r) [Cleaved into: Complement C1r subcomponent heavy chain; Complement C1r subcomponent light chain]
P02775	70.5570	45.6233	0.6466	0.0040	Platelet basic protein (PBP) (C-X-C motif chemokine 7) (Leukocyte-derived growth factor) (LDGF) (Macrophage-derived growth factor) (MDGF) (Small-inducible cytokine B7) [Cleaved into: Connective tissue-activating peptide III (CTAP-III) (LA-PF4) (Low-affinity platelet factor IV); TC-2; Connective tissue-activating peptide III(1-81) (CTAP-III(1-81)); Beta-thromboglobulin (Beta-TG); Neutrophil-activating peptide 2(74) (NAP-2(74)); Neutrophil-activating peptide 2(73) (NAP-2(73)); Neutrophil-activating peptide 2 (NAP-2); TC-1; Neutrophil-activating peptide 2(1-66) (NAP-2(1-66)); Neutrophil-activating peptide 2(1-63) (NAP-2(1-63))]
P08603	75.2708	44.0433	0.5851	0.0016	Complement factor H (H factor 1)
P02746	73.7319	37.9529	0.5147	0.0000	Complement C1q subcomponent subunit B

B. **Plasma**

Uniprot code (AC)	Healthy Median	COVID-19 Median	Fold changes (COVID-19/ Healthy)	P-value	Function
P26038	17.3506	45.4951	2.6221	0.0005	Moesin (Membrane-organizing extension spike protein)
P12814	18.1181	44.3925	2.4502	0.0039	Alpha-actinin-1 (Alpha-actinin cytoskeletal isoform) (F-actin cross-linking protein) (Non-muscle alpha-actinin-1)
Q9UIV8	16.3197	37.4158	2.2927	0.0010	Serpin B13 (HaCaT UV-repressible serpin) (Hurpin) (Headpin) (Peptidase inhibitor 13) (PI-13) (Proteinase inhibitor 13)
P61970	15.7125	35.3690	2.2510	0.0498	Nuclear transport factor 2 (NTF-2) (Placental protein 15) (PP15)
O60235	27.2652	57.5138	2.1094	0.0037	Transmembrane protease serine 11D (EC 3.4.21.-) (Airway trypsin-like protease) [Cleaved into: Transmembrane protease serine 11D non-catalytic chain; Transmembrane protease serine 11D catalytic chain]
P02533	23.8479	45.7757	1.9195	0.0002	Keratin, type I cytoskeletal 14 (Cytokeratin-14) (CK-14) (Keratin-14) (K14)

P47756	33.9481	61.7486	1.8189	0.0254	F-actin-capping protein subunit beta (CapZ beta)
P07737	23.2971	41.5104	1.7818	0.0337	Profilin-1 (Epididymis tissue protein Li 184a) (Profilin I)
O95336	37.0038	65.1229	1.7599	0.0304	6-phosphogluconolactonase (6PGL) (EC 3.1.1.31)
P31946	34.4017	60.1709	1.7491	0.0011	14-3-3 protein beta/alpha (Protein 1054) (Protein kinase C inhibitor protein 1) (KCIP-1) [Cleaved into: 14-3-3 protein beta/alpha, N-terminally processed]
Q9P1F3	29.0120	50.5459	1.7422	0.0022	Costars family protein ABRACL (ABRA C-terminal-like protein)
P04083	38.1212	64.8081	1.7001	0.0002	Annexin A1 (Annexin I) (Annexin-1) (Calpactin II) (Calpactin-2) (Chromobindin-9) (Lipocortin I) (Phospholipase A2 inhibitory protein) (p35)
P01877	38.7187	62.3788	1.6111	0.0100	Immunoglobulin heavy constant alpha 2 (Ig alpha-2 chain C region) (Ig alpha-2 chain C region BUT) (Ig alpha-2 chain C region LAN)
P01624	34.8145	55.9570	1.6073	0.0066	Immunoglobulin kappa variable 3-15 (Ig kappa chain V-III region CLL) (Ig kappa chain V-III region POM)
P04792	34.3107	55.1068	1.6061	0.0077	Heat shock protein beta-1 (HspB1) (28 kDa heat shock protein) (Estrogen-regulated 24 kDa protein) (Heat shock 27 kDa protein) (HSP 27) (Stress-responsive protein 27) (SRP27)
P03973	38.2868	61.3574	1.6026	0.0034	Antileukoproteinase (ALP) (BLPI) (HUSI-1) (Mucus proteinase inhibitor) (MPI) (Protease inhibitor WAP4) (Secretory leukocyte protease inhibitor) (Seminal proteinase inhibitor) (WAP four-disulfide core domain protein 4)
P22079	22.2845	33.7772	1.5157	0.0330	Lactoperoxidase (LPO) (EC 1.11.1.7) (Salivary peroxidase) (SPO)
Q01518	43.5573	65.9063	1.5131	0.0018	Adenylyl cyclase-associated protein 1 (CAP 1)
P14780	40.0000	59.8204	1.4955	0.0280	Matrix metalloproteinase-9 (MMP-9) (EC 3.4.24.35) (92 kDa gelatinase) (92 kDa type IV collagenase) (Gelatinase B) (GELB) [Cleaved into: 67 kDa matrix metalloproteinase-9; 82 kDa matrix metalloproteinase-9]
P61158	51.1722	74.2110	1.4502	0.0003	Actin-related protein 3 (Actin-like protein 3)
P18510	40.5000	58.6667	1.4486	0.0187	Interleukin-1 receptor antagonist protein (IL-1RN) (IL-1ra) (IRAP) (ICIL-1RA) (IL1 inhibitor) (Anakinra)
P37802	34.2496	48.8856	1.4273	0.0378	Transgelin-2 (Epididymis tissue protein Li 7e) (SM22-alpha homolog)
A0A0B4J1X5	32.2115	45.8654	1.4239	0.0020	Immunoglobulin heavy variable 3-74
P07858	45.6759	61.9913	1.3572	0.0060	Cathepsin B (EC 3.4.22.1) (APP secretase) (APPS) (Cathepsin B1) [Cleaved into: Cathepsin B light chain; Cathepsin B heavy chain]
P27482	56.7964	75.4308	1.3281	0.0179	Calmodulin-like protein 3 (CaM-like protein) (CLP) (Calmodulin-related protein NB-1)
Q01469	50.5788	66.5325	1.3154	0.0468	Fatty acid-binding protein 5 (Epidermal-type fatty acid-binding protein) (E-FABP) (Fatty acid-binding protein, epidermal) (Psoriasis-associated fatty acid-binding protein homolog) (PA-FABP)
P60709	48.5144	63.6549	1.3121	0.0368	Actin, cytoplasmic 1 (Beta-actin) [Cleaved into: Actin, cytoplasmic 1, N-terminally processed]
P07195	55.9759	70.2851	1.2556	0.0365	L-lactate dehydrogenase B chain (LDH-B) (EC 1.1.1.27) (LDH heart subunit) (LDH-H) (Renal carcinoma antigen NY-REN-46)
P07339	58.2806	71.5190	1.2271	0.0405	Cathepsin D (EC 3.4.23.5) [Cleaved into: Cathepsin D light chain; Cathepsin D heavy chain]
O15144	50.5818	61.4430	1.2147	0.0301	Actin-related protein 2/3 complex subunit 2 (Arp2/3 complex 34 kDa subunit) (p34-ARC)

Q8NFU4	54.5973	65.9801	1.2085	0.0147	Follicular dendritic cell secreted peptide (FDC secreted protein) (FDC-SP)
P55058	58.0352	68.9266	1.1877	0.0438	Phospholipid transfer protein (Lipid transfer protein II)
P0DOY2	61.4466	72.3315	1.1771	0.0478	Immunoglobulin lambda constant 2 (Ig lambda chain C region Kern) (Ig lambda chain C region NIG-64) (Ig lambda chain C region SH) (Ig lambda chain C region X) (Ig lambda-2 chain C region)
O95274	63.3065	73.1720	1.1558	0.0134	Ly6/PLAUR domain-containing protein 3 (GPI-anchored metastasis-associated protein C4.4A homolog) (Matrigel-induced gene C4 protein) (MIG-C4)
Q07654	73.2726	83.5565	1.1404	0.0019	Trefoil factor 3 (Intestinal trefoil factor) (hITF) (Polypeptide P1.B) (hP1.B)
P68871	66.2918	73.3739	1.1068	0.0398	Hemoglobin subunit beta (Beta-globin) (Hemoglobin beta chain) [Cleaved into: LVV-hemorphin-7; Spinorphin]
Q96BQ1	80.6410	72.3077	0.8967	0.0287	Protein FAM3D
P28325	88.8382	76.2557	0.8584	0.0338	Cystatin-D (Cystatin-5)
P01037	61.6983	52.8035	0.8558	0.0039	Cystatin-SN (Cystain-SA-I) (Cystatin-1) (Salivary cystatin-SA-1)
P06702	72.0779	60.3175	0.8368	0.0410	Protein S100-A9 (Calgranulin-B) (Calprotectin L1H subunit) (Leukocyte L1 complex heavy chain) (Migration inhibitory factor-related protein 14) (MRP-14) (p14) (S100 calcium-binding protein A9)
P07384	85.5193	64.5104	0.7543	0.0020	Calpain-1 catalytic subunit (EC 3.4.22.52) (Calcium-activated neutral proteinase 1) (CANP 1) (Calpain mu-type) (Calpain-1 large subunit) (Cell proliferation-inducing gene 30 protein) (Micromolar-calpain) (muCANP)
O60888	58.5434	43.0439	0.7352	0.0163	Protein CutA (Acetylcholinesterase-associated protein) (Brain acetylcholinesterase putative membrane anchor)
P50395	75.2077	51.7572	0.6882	0.0415	Rab GDP dissociation inhibitor beta (Rab GDI beta) (Guanosine diphosphate dissociation inhibitor 2) (GDI-2)
P06331	71.5901	49.0953	0.6858	0.0148	Immunoglobulin heavy variable 4-34 (Ig heavy chain V-II region ARH-77)
P06870	64.1864	40.8901	0.6371	0.0032	Kallikrein-1 (EC 3.4.21.35) (Kidney/pancreas/salivary gland kallikrein) (Tissue kallikrein)
P0DUB6	55.9848	35.3483	0.6314	0.0095	Alpha-amylase 1A (EC 3.2.1.1) (1,4-alpha-D-glucan glucanohydrolase 1) (Salivary alpha-amylase)
P05164	81.4325	48.3310	0.5935	0.0001	Myeloperoxidase (MPO) (EC 1.11.2.2) [Cleaved into: Myeloperoxidase; 89 kDa myeloperoxidase; 84 kDa myeloperoxidase; Myeloperoxidase light chain; Myeloperoxidase heavy chain]
P23141	77.4447	44.7537	0.5779	0.0042	Liver carboxylesterase 1 (Acyl-coenzyme A:cholesterol acyltransferase) (ACAT) (Brain carboxylesterase hBr1) (Carboxylesterase 1) (CE-1) (hCE-1) (EC 3.1.1.1) (Cholesteryl ester hydrolase) (CEH) (EC 3.1.1.13) (Cocaine carboxylesterase) (Egasyn) (HMSE) (Methylumbelliferyl-acetate deacetylase 1) (EC 3.1.1.56) (Monocyte/macrophage serine esterase) (Retinyl ester hydrolase) (REH) (Serine esterase 1) (Triacylglycerol hydrolase) (TGH)
P59666	65.3631	36.6480	0.5607	0.0496	Neutrophil defensin 3 (Defensin, alpha 3) (HNP-3) (HP-3) (HP3) [Cleaved into: HP 3-56; Neutrophil defensin 2 (HNP-2) (HP-2) (HP2)]
P62258	90.6659	49.5838	0.5469	0.0003	14-3-3 protein epsilon (14-3-3E)

Figure 4. Network analyses depicted biological functions altered in convalescent plasma and saliva.

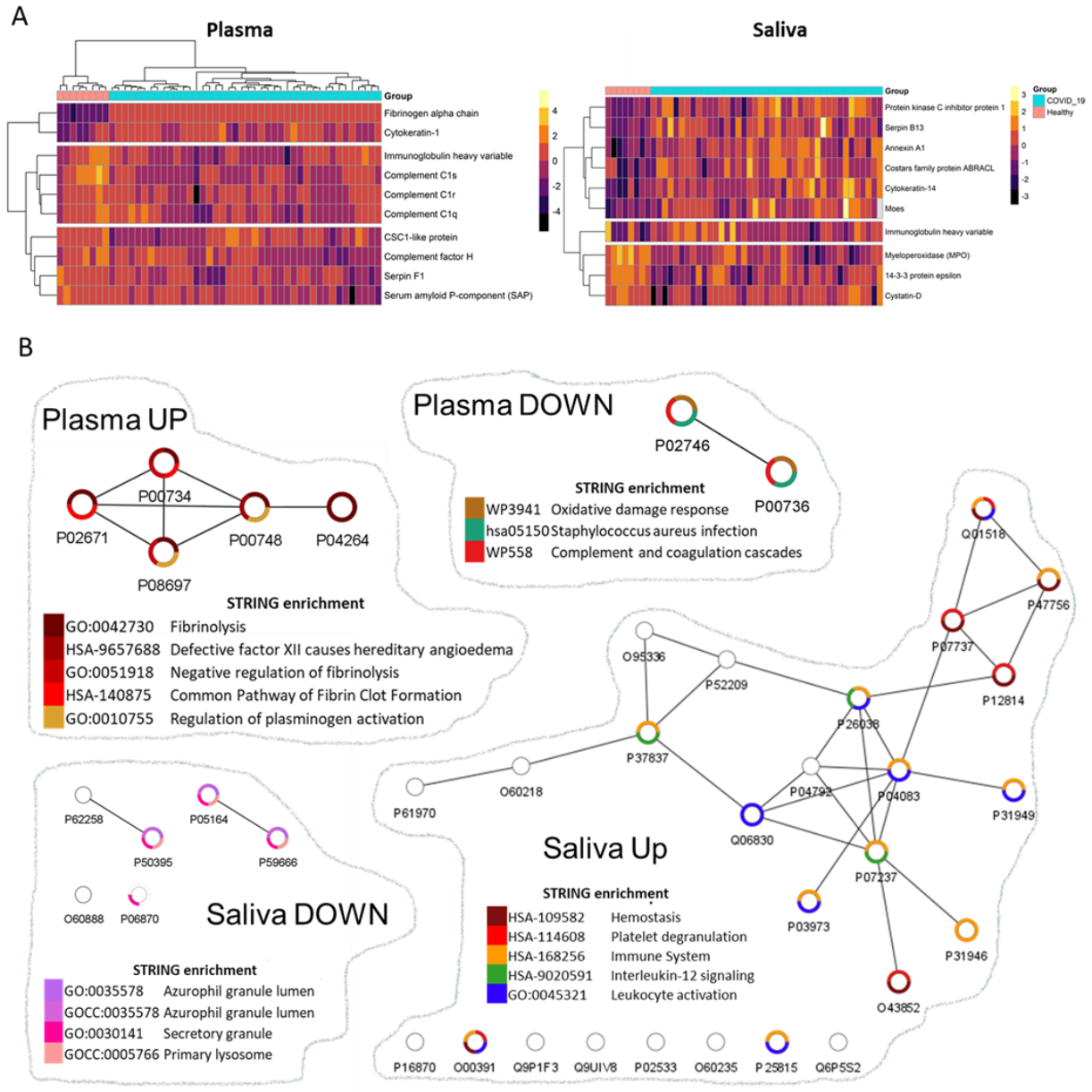

Figure 5. Comparative proteomic analyses between saliva and plasma revealed the heterologous signatures of each biofluid and further divarication of COVID-19 saliva.

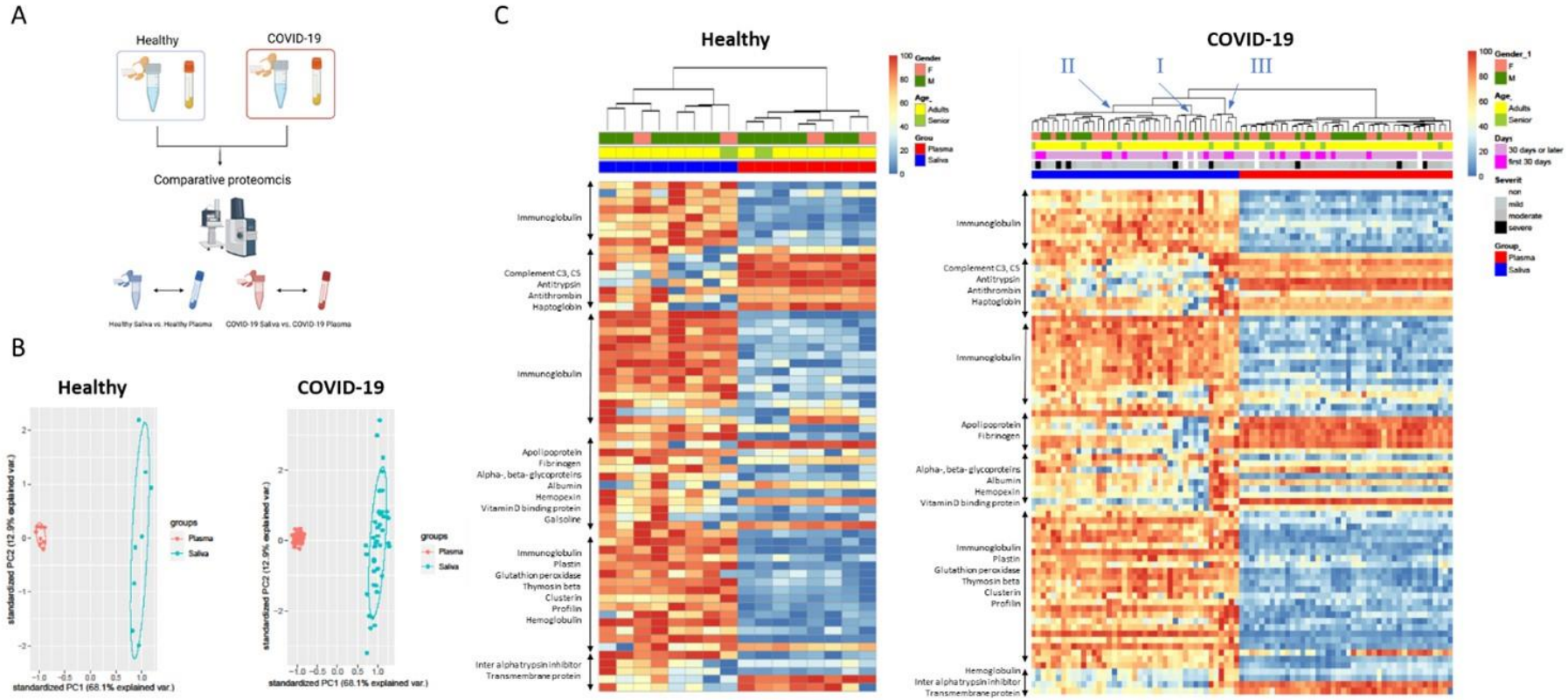

Figure 6. Correlation analyses suggests that proteomic alterations in convalescent saliva is associated with antibody responses specific to the receptor binding site (RBD) of SARS-CoV-2.

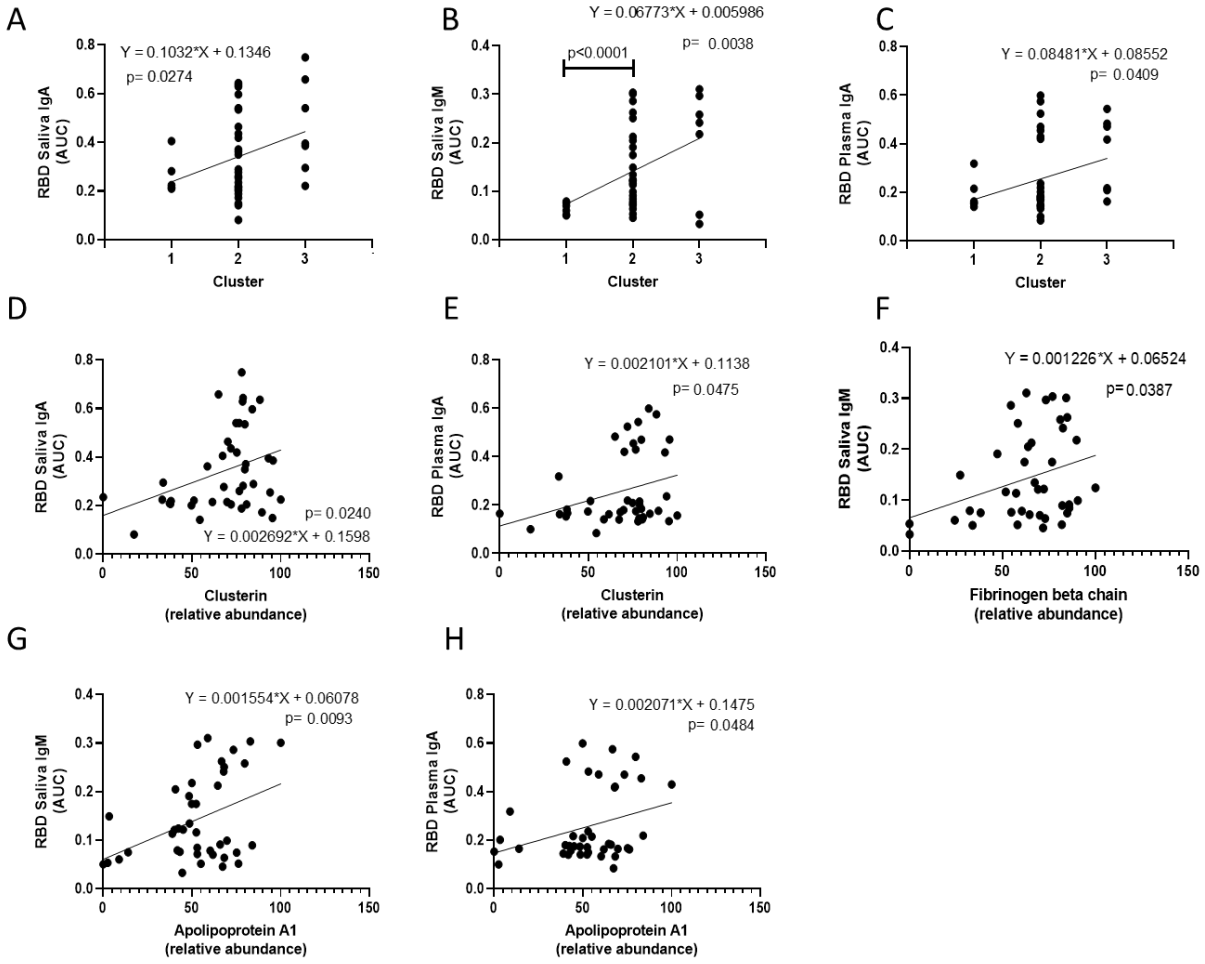

Table 2. Correlations among RBD binding immunoglobulins, fibrinogen proteins, and demographic factors.

All			
Factor A	**Factor B**	**Pearson R**	**P value**
Plasma fibrinogen alpha chain	Saliva fibrinogen beta chain	-0.051	0.033
Plasma fibrinogen alpha chain	Saliva fibrinogen gamma chain	-0.305	0.004
Plasma fibrinogen alpha chain	Saliva RBD IgA	0.406	<0.0005
Plasma fibrinogen alpha chain	Saliva RBD IgM	-0.493	0.010
Plasma fibrinogen alpha chain	Plasma RBD IgA	0.364	<0.0005
Saliva fibrinogen alpha chain	Saliva fibrinogen beta chain	0.845	<0.0005
Saliva fibrinogen beta chain	Saliva fibrinogen gamma chain	0.284	0.048
Saliva fibrinogen beta chain	Saliva RBD IgM	0.298	0.037
Saliva RBD IgA	Saliva RBD IgM	0.344	0.016
Plasma RBD IgA	Saliva RBD IgM	-0.355	0.012
Plasma RBD IgA	Seniroty (60yrs or higher)	-0.301	0.036
Categorized Disease severity	Saliva RBD IgM	-0.352	0.013
Categorized Disease severity	Days since onset of symptoms	0.468	0.003
Days since onset of symptoms	Saliva RBD IgM	-0.442	0.005
Healthy only			
Factor A	**Factor B**	**Pearson R**	**P value**
Plasma fibrinogen alpha chain	Saliva RBD IgM	-0.720	0.044
Saliva fibrinogen alpha chain	Saliva fibrinogen beta chain	0.847	0.008
Saliva fibrinogen beta chain	Saliva fibrinogen gamma chain	0.776	0.024
Saliva fibrinogen beta chain	Saliva RBD IgA	-0.887	0.003
Saliva fibrinogen beta chain	Categorized gender	-0.787	0.020
Saliva fibrinogen gamma chain	Categorized gender	-0.859	0.006
COVID-19 only			
Factor A	**Factor B**	**Pearson R**	**P value**
Saliva fibrinogen alpha chain	Saliva fibrinogen beta chain	0.917	<0.0005
Saliva fibrinogen alpha chain	Saliva RBD IgM	0.309	0.049
Saliva fibrinogen beta chain	Saliva RBD IgM	0.324	0.039
Saliva RBD IgA	Saliva RBD IgM	0.716	<0.0005
Saliva RBD IgM	Days since onset of symptoms	-0.442	0.005
Plasma RBD IgA	Seniroty (60yrs or higher)	-0.312	0.047
Categorized Disease severity	Days since onset of symptoms	0.468	0.003

REFERENCES

1. Hassan, I., Mukaigawara, M., King, L., Fernandes, G. & Sridhar, D. Hindsight is 2020? Lessons in global health governance one year into the pandemic. *Nat. Med.* **27**, 396–400 (2021).
2. Mallah, S. I. *et al.* COVID-19: breaking down a global health crisis. *Annals of Clinical Microbiology and Antimicrobials* vol. 20 (2021).
3. Smith, N. *et al.* Distinct systemic and mucosal immune responses during acute SARS-CoV-2 infection. *Nat. Immunol.* **22**, 1428–1439 (2021).
4. Sacco, K. *et al.* Immunopathological signatures in multisystem inflammatory syndrome in children and pediatric COVID-19. *Nat. Med.* (2022) doi:10.1038/s41591-022-01724-3.
5. Stephenson, E. *et al.* Single-cell multi-omics analysis of the immune response in COVID-19. *Nat. Med.* **27**, 904–916 (2021).
6. Yang, Y. *et al.* Longitudinal analysis of antibody dynamics in COVID-19 convalescents reveals neutralizing responses up to 16 months after infection. *Nat Microbiol* **7**, 423–433 (2022).
7. Krammer, F. SARS-CoV-2 vaccines in development. *Nature* **586**, 516–527 (2020).
8. Kundu, R. *et al.* Cross-reactive memory T cells associate with protection against SARS-CoV-2 infection in COVID-19 contacts. *Nat. Commun.* **13**, 80 (2022).
9. Bertoletti, A., Le Bert, N., Qui, M. & Tan, A. T. SARS-CoV-2-specific T cells in infection and vaccination. *Cell. Mol. Immunol.* **18**, 2307–2312 (2021).
10. Ng, H. *et al.* Circulating Markers of Neutrophil Extracellular Traps Are of Prognostic Value in Patients With COVID-19. *Arterioscler. Thromb. Vasc. Biol.* **41**, 988–994 (2021).
11. Sui, J., Noubouossie, D. F., Gandotra, S. & Cao, L. Elevated Plasma Fibrinogen Is

Associated With Excessive Inflammation and Disease Severity in COVID-19 Patients. *Front. Cell. Infect. Microbiol.* **11**, 734005 (2021).

12. Bi, X. *et al.* Prediction of severe illness due to COVID-19 based on an analysis of initial Fibrinogen to Albumin Ratio and Platelet count. *Platelets* **31**, 674–679 (2020).
13. Chandel, A. *et al.* Association of D-dimer and Fibrinogen With Hypercoagulability in COVID-19 Requiring Extracorporeal Membrane Oxygenation. *J. Intensive Care Med.* **36**, 689–695 (2021).
14. Gillot, C. *et al.* NETosis and the Immune System in COVID-19: Mechanisms and Potential Treatments. *Front. Pharmacol.* **12**, 708302 (2021).
15. Borges, L., Pithon-Curi, T. C., Curi, R. & Hatanaka, E. COVID-19 and Neutrophils: The Relationship between Hyperinflammation and Neutrophil Extracellular Traps. *Mediators Inflamm.* **2020**, 8829674 (2020).
16. Davis, H. E. *et al.* Characterizing long COVID in an international cohort: 7 months of symptoms and their impact. *EClinicalMedicine* **38**, 101019 (2021).
17. Fenstemacher, P. A. & Winn, P. *Post-Acute and Long-Term Medicine: A Pocket Guide*. (Humana Press, 2015).
18. Phetsouphanh, C. *et al.* Immunological dysfunction persists for 8 months following initial mild-to-moderate SARS-CoV-2 infection. *Nature Immunology* vol. 23 210–216 (2022).
19. Su, Y. *et al.* Multiple early factors anticipate post-acute COVID-19 sequelae. *Cell* **185**, 881–895.e20 (2022).
20. Long COVID and kids: more research is urgently needed. *Nature* **602**, 183 (2022).
21. Meringer, H. *et al.* DOP19 Myeloid and lymphoid cell abnormalities persist in the intestinal mucosa of patients who recover from COVID-19 infection. *J. Crohns. Colitis* **16**, i068–i069 (2022).
22. Proal, A. D. & VanElzakker, M. B. Long COVID or Post-acute Sequelae of COVID-19 (PASC): An Overview of Biological Factors That May Contribute to Persistent Symptoms.

Front. Microbiol. **12**, 698169 (2021).

23. Liu, Q. *et al.* Gut microbiota dynamics in a prospective cohort of patients with post-acute COVID-19 syndrome. *Gut* **71**, 544–552 (2022).
24. Hirschenberger, M., Hunszinger, V. & Sparrer, K. M. J. Implications of Innate Immunity in Post-Acute Sequelae of Non-Persistent Viral Infections. *Cells* **10**, (2021).
25. Huang, N. *et al.* SARS-CoV-2 infection of the oral cavity and saliva. *Nat. Med.* **27**, 892–903 (2021).
26. Brandtzaeg, P. Secretory immunity with special reference to the oral cavity. *J. Oral Microbiol.* **5**, (2013).
27. Siqueira, W. L., Salih, E., Wan, D. L., Helmerhorst, E. J. & Oppenheim, F. G. Proteome of human minor salivary gland secretion. *J. Dent. Res.* **87**, 445–450 (2008).
28. Zenobia, C., Herpoldt, K.-L. & Freire, M. Is the oral microbiome a source to enhance mucosal immunity against infectious diseases? *NPJ Vaccines* **6**, 80 (2021).
29. Brandini, D. A. *et al.* Covid-19 and oral diseases: Crosstalk, synergy or association? *Rev. Med. Virol.* **31**, e2226 (2021).
30. Hasturk, H., Kantarci, A. & Van Dyke, T. E. Oral inflammatory diseases and systemic inflammation: role of the macrophage. *Front. Immunol.* **3**, 118 (2012).
31. Heron, S. E. & Elahi, S. HIV Infection and Compromised Mucosal Immunity: Oral Manifestations and Systemic Inflammation. *Front. Immunol.* **8**, 241 (2017).
32. Marouf, N. *et al.* Association between periodontitis and severity of COVID-19 infection: A case-control study. *J. Clin. Periodontol.* **48**, 483–491 (2021).
33. Tsunetsugu-Yokota, Y. *et al.* Saliva as a useful tool for evaluating upper mucosal antibody response to influenza. *PLoS One* **17**, e0263419 (2022).
34. de Silva, H. V. *et al.* Purification and characterization of apolipoprotein J. *J. Biol. Chem.* **265**, 14292–14297 (1990).
35. Vidarsson, G., Dekkers, G. & Rispens, T. IgG subclasses and allotypes: from structure to

effector functions. *Front. Immunol.* **5**, 520 (2014).

36. Matsumoto, M. & Hirata, T. Moesin regulates neutrophil rolling velocity in vivo. *Cell. Immunol.* **304-305**, 59–62 (2016).
37. Liu, X. *et al.* Moesin and myosin phosphatase confine neutrophil orientation in a chemotactic gradient. *J. Exp. Med.* **212**, 267–280 (2015).
38. Yürüker, B. & Niggli, V. Alpha-actinin and vinculin in human neutrophils: reorganization during adhesion and relation to the actin network. *J. Cell Sci.* **101 (Pt 2)**, 403–414 (1992).
39. Choi, Y. J. *et al.* SERPINB1-mediated checkpoint of inflammatory caspase activation. *Nat. Immunol.* **20**, 276–287 (2019).
40. Perretti, M. & Flower, R. J. Annexin 1 and the biology of the neutrophil. *J. Leukoc. Biol.* **76**, 25–29 (2004).
41. Perretti, M. & Solito, E. Annexin 1 and neutrophil apoptosis. *Biochem. Soc. Trans.* **32**, 507–510 (2004).
42. Sehnert, B. *et al.* Antileukoproteinase: modulation of neutrophil function and therapeutic effects on anti-type II collagen antibody-induced arthritis. *Arthritis Rheum.* **50**, 2347–2359 (2004).
43. Heissig, B. *et al.* Role of neutrophil-derived matrix metalloproteinase-9 in tissue regeneration. *Histol. Histopathol.* **25**, 765–770 (2010).
44. Gelzo, M. *et al.* Matrix metalloproteinases (MMP) 3 and 9 as biomarkers of severity in COVID-19 patients. *Sci. Rep.* **12**, 1212 (2022).
45. Lan, T. *et al.* The functional prediction of transmembrane serine protease 2 (TMPRSS2) in priming S-protein of SARS-CoV-2 among vertebrates. doi:10.22541/au.159225464.44600406.
46. Berdowska, I. & Matusiewicz, M. Cathepsin L, transmembrane peptidase/serine subfamily member 2/4, and other host proteases in COVID-19 pathogenesis - with impact on gastrointestinal tract. *World J. Gastroenterol.* **27**, 6590–6600 (2021).

47. Peñaloza, H. F., Lee, J. S. & Ray, P. Neutrophils and lymphopenia, an unknown axis in severe COVID-19 disease. *PLoS Pathog.* **17**, e1009850 (2021).

48. Ackermann, M. *et al.* Patients with COVID-19: in the dark-NETs of neutrophils. *Cell Death Differ.* **28**, 3125–3139 (2021).

49. Tomar, B., Anders, H.-J., Desai, J. & Mulay, S. R. Neutrophils and Neutrophil Extracellular Traps Drive Necroinflammation in COVID-19. *Cells* **9**, (2020).

50. Paludan, S. R. & Mogensen, T. H. Innate immunological pathways in COVID-19 pathogenesis. *Sci Immunol* **7**, eabm5505 (2022).

51. Cervia, C. *et al.* Immunoglobulin signature predicts risk of post-acute COVID-19 syndrome. *Nat. Commun.* **13**, 1–12 (2022).

52. Caspersen, I. H., Magnus, P. & Trogstad, L. Excess risk and clusters of symptoms after COVID-19 in a large Norwegian cohort. *bioRxiv* (2021) doi:10.1101/2021.10.15.21265038.

53. Tleyjeh, I. M. *et al.* Prevalence and predictors of Post-Acute COVID-19 Syndrome (PACS) after hospital discharge: A cohort study with 4 months median follow-up. *PLoS One* **16**, e0260568 (2021).

54. Huckriede, J. *et al.* Evolution of NETosis markers and DAMPs have prognostic value in critically ill COVID-19 patients. *Sci. Rep.* **11**, 15701 (2021).

55. Arcanjo, A. *et al.* The emerging role of neutrophil extracellular traps in severe acute respiratory syndrome coronavirus 2 (COVID-19). *Sci. Rep.* **10**, 19630 (2020).

56. Varjú, I. & Kolev, K. Networks that stop the flow: A fresh look at fibrin and neutrophil extracellular traps. *Thromb. Res.* **182**, 1–11 (2019).

57. Silva, L. M. *et al.* Fibrin is a critical regulator of neutrophil effector function at mucosal barrier sites. *bioRxiv* 2021.01.15.426743 (2021) doi:10.1101/2021.01.15.426743.

58. Aleyd, E. *et al.* IgA Enhances NETosis and Release of Neutrophil Extracellular Traps by Polymorphonuclear Cells via Fcα Receptor I. *The Journal of Immunology* vol. 192 2374–2383 (2014).

59. Chen, X.-Q. *et al.* The Involvement of Neutrophil Extracellular Traps in Disease Activity Associated With IgA Vasculitis. *Front. Immunol.* **12**, 668974 (2021).

60. Heineke, M. H. *et al.* New insights in the pathogenesis of immunoglobulin A vasculitis (Henoch-Schönlein purpura). *Autoimmun. Rev.* **16**, 1246–1253 (2017).

61. Li, Q. *et al.* Neutrophil-to-lymphocyte ratio as an independent inflammatory indicator of poor prognosis in IgA nephropathy. *Int. Immunopharmacol.* **87**, 106811 (2020).

62. Stacey, H. D. *et al.* IgA potentiates NETosis in response to viral infection. *Proc. Natl. Acad. Sci. U. S. A.* **118**, (2021).

63. Pang, N. Y.-L., Pang, A. S.-R., Chow, V. T. & Wang, D.-Y. Understanding neutralising antibodies against SARS-CoV-2 and their implications in clinical practice. *Mil Med Res* **8**, 47 (2021).

64. Wang, Z. *et al.* Enhanced SARS-CoV-2 neutralization by dimeric IgA. *Sci. Transl. Med.* **13**, (2021).

65. Saito, S. *et al.* IgA tetramerization improves target breadth but not peak potency of functionality of anti-influenza virus broadly neutralizing antibody. *PLoS Pathog.* **15**, e1007427 (2019).

66. Sun, L. *et al.* Increased in vitro neutralizing activity of SARS-CoV-2 IgA1 dimers compared to monomers and IgG. *Proc. Natl. Acad. Sci. U. S. A.* **118**, (2021).

67. Sterlin, D. *et al.* IgA dominates the early neutralizing antibody response to SARS-CoV-2. *Sci. Transl. Med.* **13**, (2021).

68. Stolovich-Rain, M. *et al.* Intramuscular mRNA BNT162b2 vaccine against SARS-CoV-2 induces robust neutralizing salivary IgA. *bioRxiv* 2022.02.17.480851 (2022) doi:10.1101/2022.02.17.480851.

69. Stadnytskyi, V., Anfinrud, P. & Bax, A. Breathing, speaking, coughing or sneezing: What drives transmission of SARS-CoV-2? *J. Intern. Med.* **290**, 1010–1027 (2021).

70. Beyene, G. T. *et al.* Saliva is superior over nasopharyngeal swab for detecting SARS-CoV2

in COVID-19 patients. *Sci. Rep.* **11**, 22640 (2021).

71. Yan, X. *et al.* A cross-sectional study of the epidemic situation on COVID-19 in Gansu Province, China - a big data analysis of the national health information platform. *BMC Infect. Dis.* **21**, 146 (2021).

72. Yu Y, Sikorski P, Smith M, Bowman-Gholston C, Cacciabeve N, Nelson KE, et al. Comprehensive Metaproteomic Analyses of Urine in the Presence and Absence of Neutrophil-Associated Inflammation in the Urinary Tract. *Theranostics*. **7**(2):238–252 (2017).

73. Whitt, M. A. Generation of VSV pseudotypes using recombinant ΔG-VSV for studies on virus entry, identification of entry inhibitors, and immune responses to vaccines. *J. Virol. Methods* **169**, 365–374 (2010).

74. Lei, C., Yang, J., Hu, J. & Sun, X. On the Calculation of TCID50 for Quantitation of Virus Infectivity. *Virol. Sin.* **36**, 141–144 (2021).

75. Nie, J. *et al.* Quantification of SARS-CoV-2 neutralizing antibody by a pseudotyped virus-based assay. *Nat. Protoc.* **15**, 3699–3715 (2020).

76. Reed, L. J. & Muench, H. A SIMPLE METHOD OF ESTIMATING FIFTY PER CENT ENDPOINTS12. *American Journal of Epidemiology* vol. 27 493–497 (1938).

77. Yu, Y. *et al.* Comprehensive Metaproteomic Analyses of Urine in the Presence and Absence of Neutrophil-Associated Inflammation in the Urinary Tract. *Theranostics* **7**, 238–252 (2017).

78. Cantwell, A. M. *et al.* Kinetic Multi-omic Analysis of Responses to SARS-CoV-2 Infection in a Model of Severe COVID-19. *J. Virol.* **95**, e0101021 (2021).

79. Shannon, P. *et al.* Cytoscape: a software environment for integrated models of biomolecular interaction networks. *Genome Res.* **13**, 2498–2504 (2003).

80. Team, R. C. & Others. R: A language and environment for statistical computing. (2013).

81. Lau WW, Hardt M, Zhang YH, Freire M, Ruhl S. The Human Salivary Proteome Wiki: A Community-Driven Research Platform. *J Dent Res*. **100**(13):1510–9 (2021).